Supporting Information

A hydrogel thermoelectrochemical cell with high self-healability and enhanced thermopower dually induced by zwitterion

Youfa Liu,[1] Li Yin,[1] Sheng Chen,[1,3] Yao Liu,[1,2] Qingjiang Liu,[1,2] Liangliang Yang,[1,2] Yingchun Li,[4] Qian Zhang,[1*] Yan Huang[1,2*]

1. The State Key Laboratory of Advanced Welding and Joining, School of Materials Science and Engineering, Harbin Institute of Technology, Shenzhen, 518055, People's Republic of China.

2. Sauvage Laboratory for Smart Materials, Shenzhen Key Laboratory of Flexible Printed Electronics Technology, School of Materials Science and Engineering, Harbin Institute of Technology, Shenzhen, 518055, People's Republic of China.

3. The Key Laboratory of Radiation Physics and Technology of Ministry of Education, Institute of Nuclear Science and Technology, Sichuan University, Chengdu, 610064, People's Republic of China.

4. School of Science, Harbin Institute of Technology, Shenzhen, 518055, People's Republic of China.

Note S1: Molecular dynamics simulation

The solvation structures of $Fe(CN)_6^{3-}$ and $Fe(CN)_6^{4-}$ were simulated by molecular dynamics (MD) performed via GROMACS 2021 software package.[1-3] $Fe(CN)_6^{3-}$ and $Fe(CN)_6^{4-}$ were modelled by all-atom force fields developed by Giacomo et al.[4] The force field parameters were taken from ref.[5] for K^+ ions. The SPC/Fw model,[6] which is capable of taking into account water flexibility,[4] was adopted for water. Furthermore, the force field parameters for PSBMA were based on the OPLS model.[7, 8] The number of ions/molecules is summarized in Table S4 for all studied simulation systems.

The steepest descent method was applied to minimize the initial energy for each system with a force tolerance of 1 kJ/(mol^{-1} nm^{-1}) and a maximum step size of 0.002 ps before MD calculations.[8] In all the three directions, periodic boundary conditions were imposed. Leapfrog algorithm was used to integrate the Newtonian equation of motion. The MD simulation was processed in an NPT ensemble and the simulation time was 20 ns.

In NPT simulations, the pressure was maintained at 1 bar by the Berendsen barostat in an isotropic manner[9] and the temperature was maintained by the V-rescale thermostat at 298.15 K. The Particle-Mesh-Ewald (PME) with a fourth-order interpolation was used to evaluate the electrostatic interactions and the grid spacing was 1.0 Å,[10] whereas a cutoff of 1.4 nm was employed to calculate the short-range van der Waals interactions.

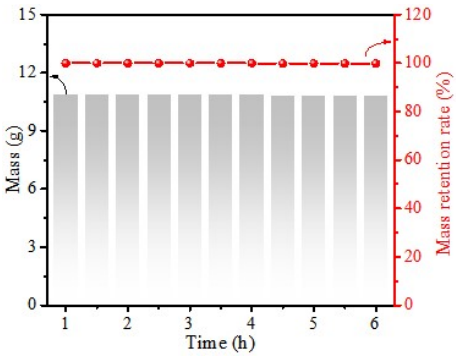

Fig. S1 Weight evolution of cling-film-encapsulated 1.8 M LiCl-0.45/0.3 M $Fe(CN)_6^{4-/3-}$-PP1 hydrogel being continuously heated at 50 °C.

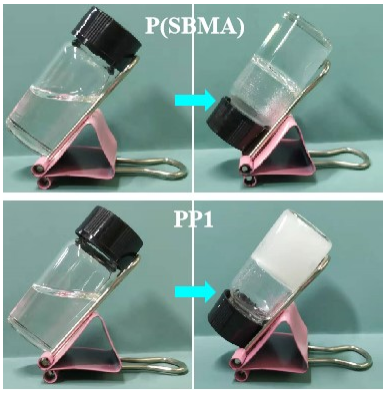

Fig. S2 Photographs of the P(SBMA) (top) and PP1 (down) hydrogels before and after polymerization.

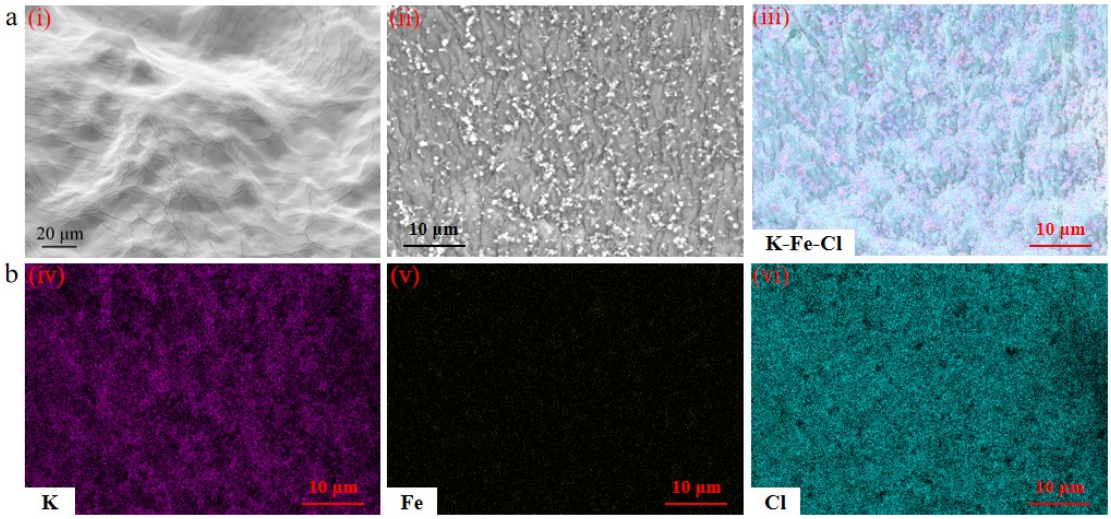

Fig. S3 SEM images PP1 hydrogel (i), 1.8 M LiCl-0.45/0.3 M $Fe(CN)_6^{4-/3-}$-PP1 hydrogel at the cross-section (ii) and its corresponding elemental mapping images of K-Fe-Cl (iii), K (iv), Fe (v) and Cl (vi).

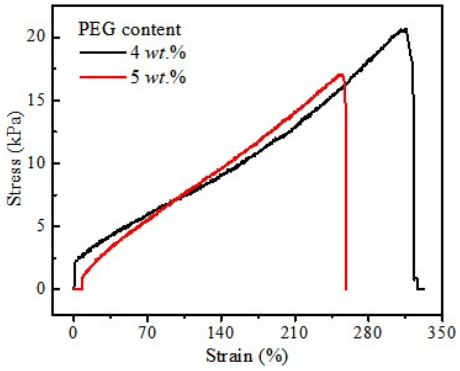

Fig. S4 Stress-strain curves of P(SBMA)/PEG hydrogels with 4*wt.*% and 5*wt.*% of PEG.

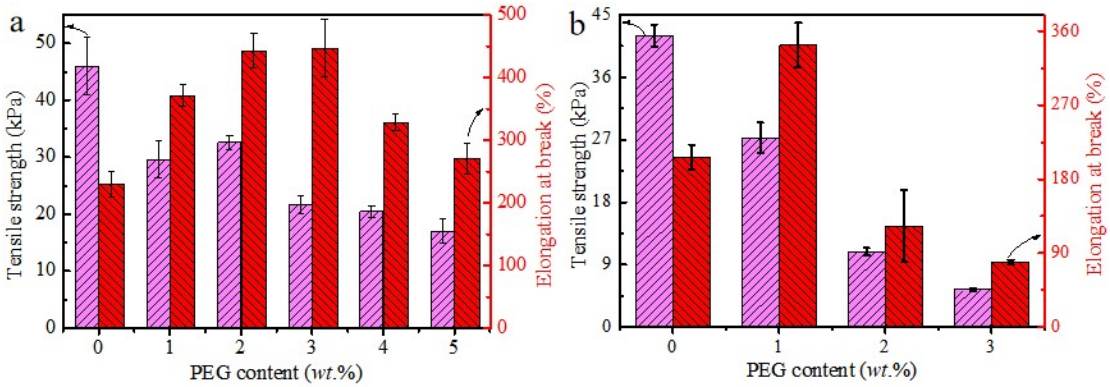

Fig. S5 Breaking strength and elongation at break of P(SBMA)/PEG hydrogels (a) before and (b) after self-healing, where the hydrogels contain different content of PEG.

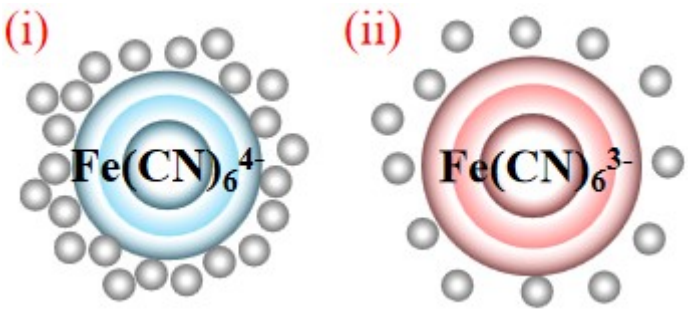

Fig. S6 The schematic hydration structures of (i) $Fe(CN)_6^{4-}$ and (ii) $Fe(CN)_6^{3-}$ in water solution according to molecular dynamics simulation.

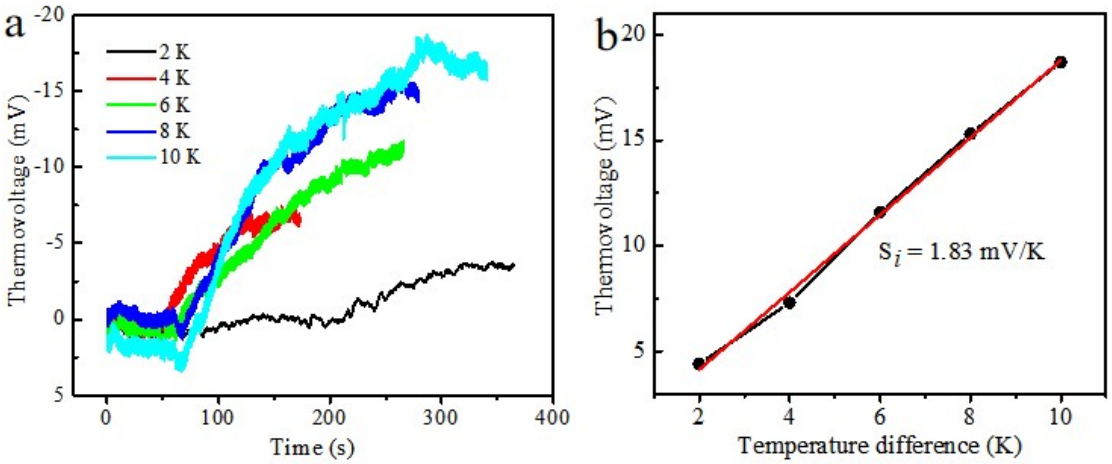

Fig. S7 (a) Thermovoltage of 1.8 M LiCl-PP1 hydrogel at different ΔT and (b) the corresponding thermopower.

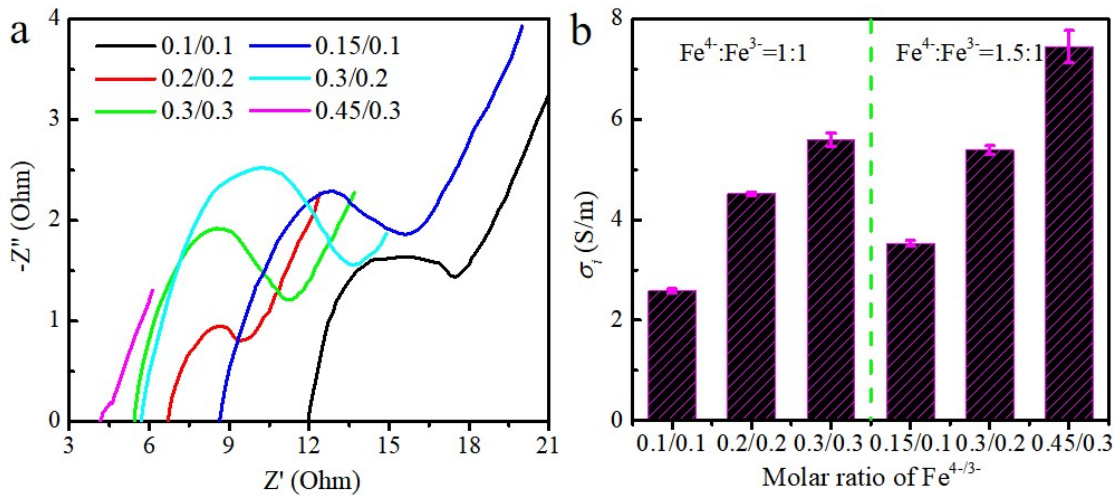

Fig. S8 (a) Nyquist diagrams, (b) ionic conductivity of the $Fe(CN)_6^{4-/3-}$-PP1 hydrogels containing redox couple with different concentration and ratio.

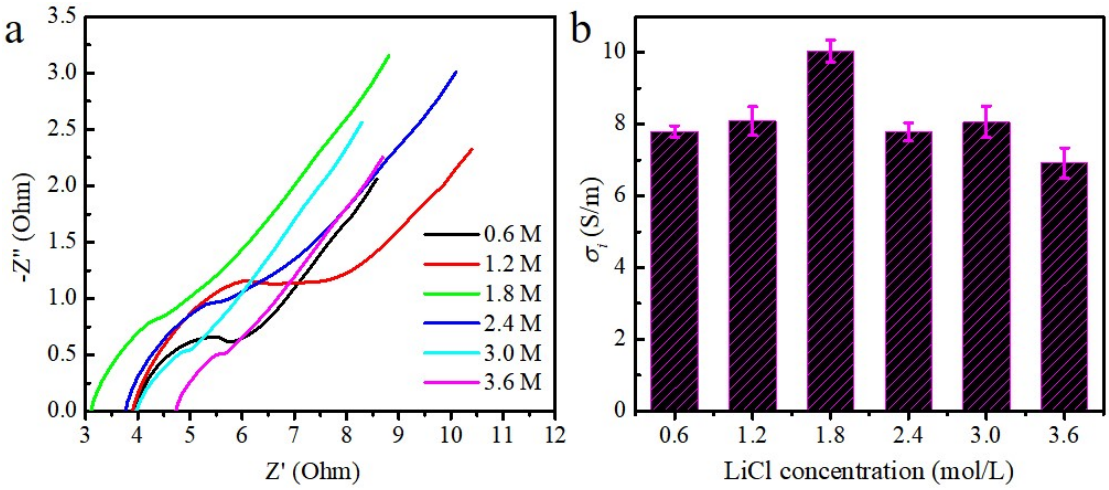

Fig. S9 (a) Nyquist diagrams, (b) ionic conductivity of the LiCl-0.45/0.3 M $Fe(CN)_6^{4-/3-}$-PP1 hydrogels containing different LiCl concentration.

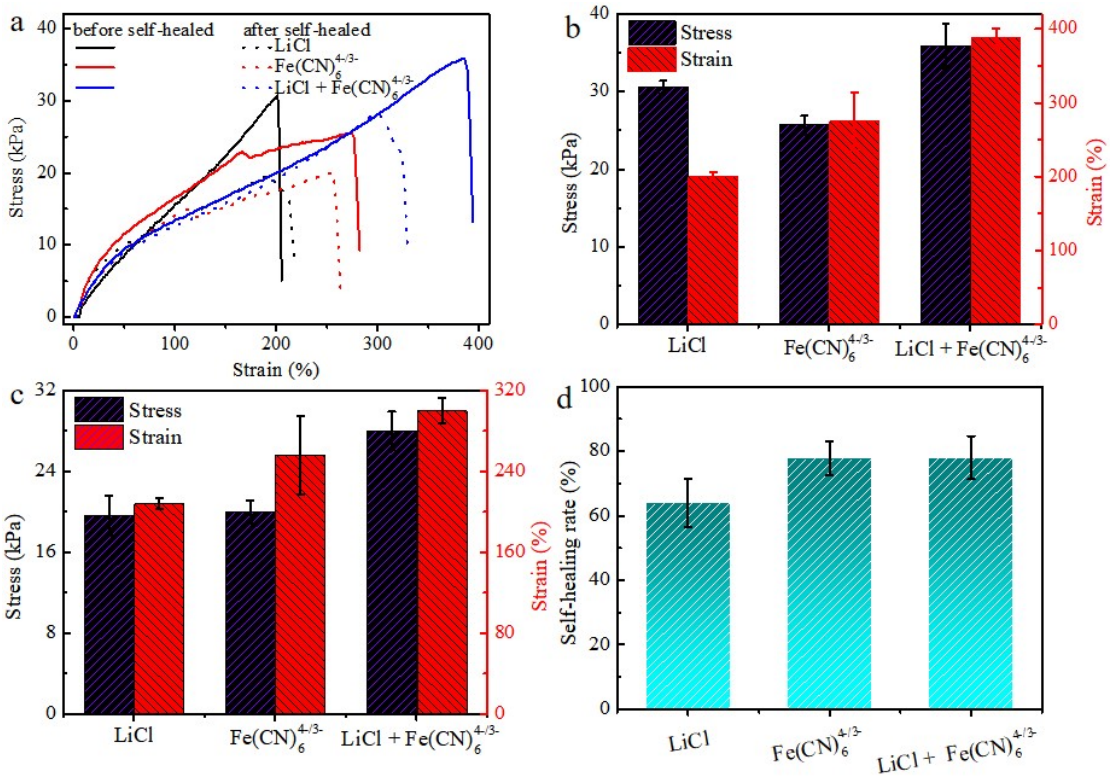

Fig. S10 (a) Stress-strain curves of 1.8 M LiCl-PP1, 0.45/0.3 M $Fe(CN)_6^{4-/3-}$-PP1 and 1.8 M LiCl-0.45/0.3 M $Fe(CN)_6^{4-/3-}$-PP1 hydrogels before and after self-healing. Breaking strength and elongation at break of 1.8 M LiCl-PP1, 0.45/0.3 M $Fe(CN)_6^{4-/3-}$-PP1 and 1.8 M LiCl-0.45/0.3 M $Fe(CN)_6^{4-/3-}$-PP1 hydrogels (b) before and (c) after self-healing. (d) Self-healing rate of 1.8 M LiCl-PP1, 0.45/0.3 M $Fe(CN)_6^{4-/3-}$-PP1 and 1.8 M LiCl-0.45/0.3 M $Fe(CN)_6^{4-/3-}$-PP1 hydrogels.

Temperature	PP1	$Fe(CN)_6^{4-/3-}$	LiCl + $Fe(CN)_6^{4-/3-}$
25 °C		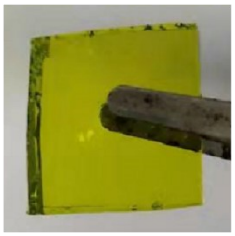	
-10 °C	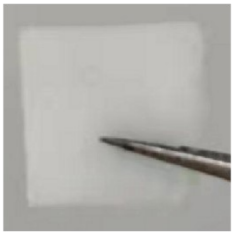	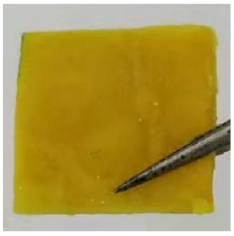	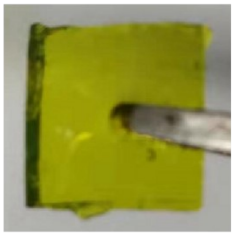

Fig. S11 Photographs of PP1, 0.45/0.3 M $Fe(CN)_6^{4-/3-}$-PP1 and 1.8 M LiCl-0.45/0.3 M $Fe(CN)_6^{4-/3-}$-PP1 hydrogels at 25 °C and -10 °C.

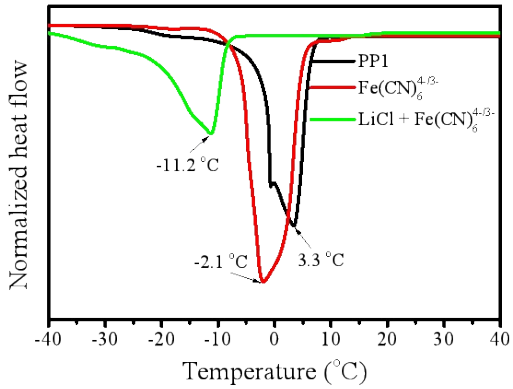

Fig. S12 DSC of PP1, 0.45/0.3 M $Fe(CN)_6^{4-/3-}$-PP1 and 1.8 M LiCl-0.45/0.3 M $Fe(CN)_6^{4-/3-}$-PP1 hydrogels.

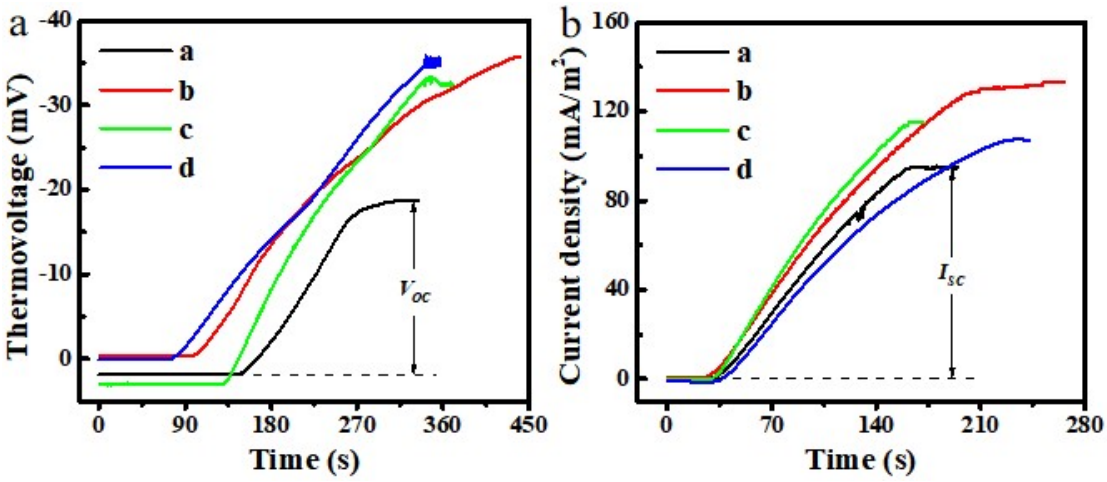

Fig. S13 (a) Open circuit voltage and (b) short circuit current of the as-prepared hybrid hydrogel with 10 K of *ΔT*. Herein, a, b, c and d are 0.45/0.3 M $Fe(CN)_6^{4-/3-}$-PP1, 1.8 M LiCl-0.45/0.3 M $Fe(CN)_6^{4-/3-}$-PP1 with or without self-healing, after 50% stretch of 1.8 M LiCl-0.45/0.3 M $Fe(CN)_6^{4-/3-}$-PP1 with self-healing, respectively.

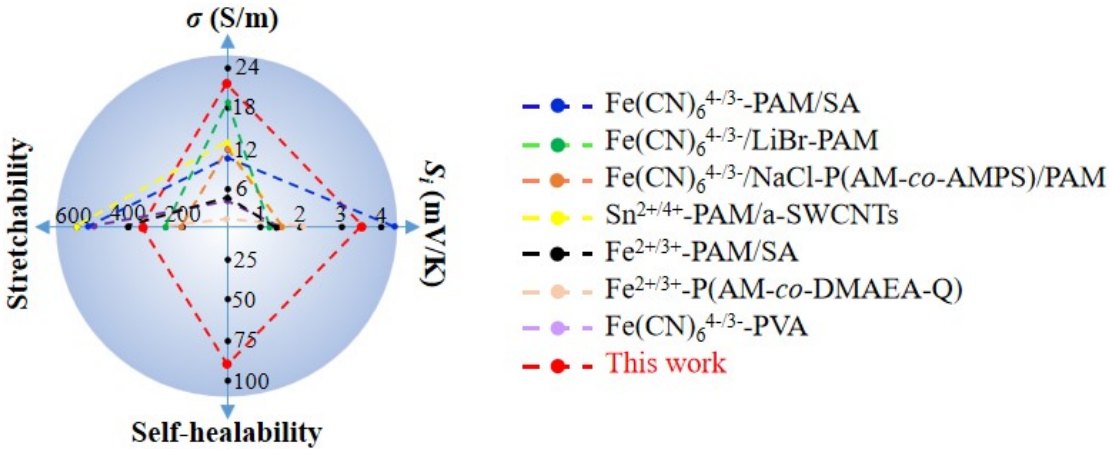

Fig. S14 Comparison of the hybrid hydrogel thermocell with previous reports in terms of thermopower, ionic conductivity, stretchability and self-healability.[11-17]

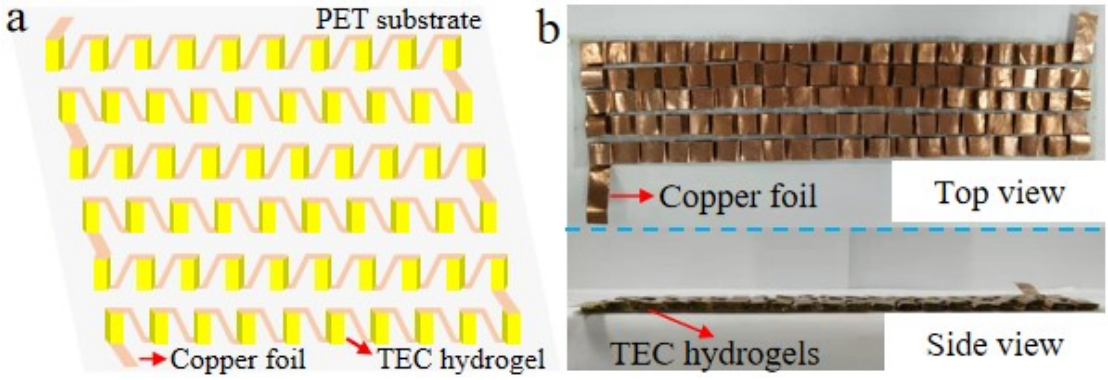

Fig. S15 Schematic illustration of the assembly of wearable thermocells array converter (a), photograph of the assembled wearable thermocells array converter (b).

Table S1 The theoretical solid and water content of P(SBMA)/PEG hybrid hydrogels with different content of PEG.

PEG content (*wt.*%)	0	1	2	3	4	5
solid content (*wt.*%)	53.3	48.6	46.1	43.5	40.2	37.8
H_2O content (*wt.*%)	46.7	51.4	53.9	56.5	59.8	62.2

Table S2 The atomic content of 1.8 M LiCl-0.45/0.3 M $Fe(CN)_6^{4-/3-}$-PP1 hydorgel at its cross-section.

PEG content (*wt.*%)	Fe	Cl	K
atomic content (at.%)	4.5	48.6	51.0

Table S3 Thermopower of state-of-the-art $Fe^{2+/3+}$-based and $Fe(CN)_6^{3-/4-}$-based thermocells.

Thermocells	S_{tg} (mV/K)	S_{td} (mV/K)	total S_t (mV/K)	contribution of S_{td} (%)	*Ref.*
gel-based LiCl-$Fe(CN)_6^{3-/4-}$	1.6	1.9	3.5	54.3	this work
gel-based $Fe^{2+/3+}$	1.43	0	1.43	0	17
gel-based $Fe^{2+/3+}$	2.02	0	2.02	0	13
gel-based $Fe(CN)_6^{3-/4-}$	1.4	0	1.4	0	18
gel-based $Fe(CN)_6^{3-/4-}$	1.5	0	1.5	0	14
gel-based $Fe(CN)_6^{3-/4-}$	4.4	0	4.4	0	12
gel-based NaCl-$Fe(CN)_6^{3-/4-}$	1.5	0.1	1.6	6.2	11
gel-based NaCl-$Fe(CN)_6^{3-/4-}$	1.4	0.36	1.76	20.4	19
gel-based KCl-$Fe(CN)_6^{3-/4-}$	2.27	14.73	17	86.6	20
gel-based KCl-$Fe(CN)_6^{3-/4-}$	4.67	20.03	24.7	81.1	21
aqueous $Fe(CN)_6^{3-/4-}$	3.7	0	3.7	0	22
aqueous $Fe(CN)_6^{3-/4-}$	4.2	0	4.2	0	23

Note: S_t is the total thermopower of thermocells, S_{tg} is the thermopower resulting from redox reaction of redox couple, S_{td} is the thermopower resulting from ionic-thermoelectrics.

Table S4 The number of ions/molecules for all studied simulation systems.

$Fe(CN)_6^{4-}$	$Fe(CN)_6^{3-}$	K^+	water	P(SBMA)	Box size (nm^3)
45		180	5556		6×6×6
	30	90	5556		6×6×6
45		180	5556	40	10×10×10
	30	90	5556	40	10×10×10

Reference

[1] Spoel D V D, Lindahl E, Hess B. GROMACS: fast, flexible, and free. *J. Comput. Chem.*, 2005;26(16):1701-1718.

[2] Abraham, et al. GROMACS: high performance molecular simulations through multi-level parallelism from laptops to supercomputers. *Soft ware X*. 2015;1-2:19-25.

[3]Berendsen H J C, van der Spoel D, van Drunen R. GROMACS: A message-passing parallel molecular dynamics implementation. *Comp. Phys. Comm.*, 1995;91:43-56.

[4] Prampolini, G. et al. Structure and dynamics of ferrocyanide and ferricyanide anions in water and heavy water: An insight by MD simulations and 2D IR Spectroscopy. *J. Phys. Chem. B*, 2014;118:899-912.

[5] Åqvist, J. Ion-water interaction potentials derived from free energy perturbation simulations. *J. Phys. Chem.*,1990; 94:8021-8024.

[6] Wu Y, Tepper H L, Voth G A. Flexible simple point-charge water model with improved liquid-state properties. *J. Chem. Phys.*,2006;124:024503.

[7] Jorgensen W L, Maxwell D S, Tirado-Rives J. Development and testing of the OPLS all-atom force field on conformational energetics and properties of organic liquids. *J. Am. Chem. Soc.*, 1996; 118:11225-11236.

[8] Vanzi F, Madan B, Sharp K. Effect of the protein denaturants urea and guanidinium on water structure: A structural and thermodynamic study. *J. Am. Chem. Soc.*,1998;120:10748-10753.

[9] Van Gunsteren W F, Berendsen H. A leap-frog algorithm for stochastic dynamics. *Mol. Simul.*, 1988;1(3):173-185.

[10]Hess B, Bekker H, Berendsen H J, Fraaije J G. LINCS: a linear constraint solver for molecular simulations. *J. Comput. Chem.*, 1997;18 (12):1463-1472.

[11] Lei Z Y, Gao W, Wu P Y. Double-network thermocells with extraordinary toughness and boosted power density for continuous heat harvesting. *Joule*. 2021;5(8):2211-2222.

[12] Zhang D, Mao Y, Ye F, Li Q, Bai PJ, He W, et al. Stretchable thermogalvanic hydrogel thermocell with record-high specific output power density enabled by ion-induced crystallization. *Energ. Environ. Sci.* 2022;15(7):2974-2982.

[13] Gao W, Lei Z Y, Zhang C B, Liu X D, Chen Y P. Stretchable and freeze-tolerant organohydrogel thermocells with enhanced thermoelectric performance continually working at subzero temperatures. *Adv. Funct. Mater.* 2021;31(43):2104071.

[14] Gao W, Lei Z Y, Chen W W, Chen Y P. Hierarchically anisotropic networks to decouple mechanical and ionic properties for high-performance quasi-solid thermocells. *ACS Nano*. 2022;16(5):8347-8357.

[15] Liang L R, Lv H C, Shi X L, Liu Z X, Chen G M, Chen Z G. A flexible quasi-solid-state thermoelectrochemical cell with high stretchability as an energy-autonomous strain sensor. *Mater. Horiz.* 2021;8(10):2750-2760.

[16] Pu S R, Liao Y T, Chen K L, Fu J, Zhang S L, Ge L R. Thermogalvanic hydrogel for synchronous evaporative cooling and low-grade heat energy harvesting. *Nano Lett.* 2020;20(5):3791-3797.

[17] Peng P, Zhou J Q, Liang L R, Huang X, Lv H C, Liu Z X. Regulating thermogalvanic effect and mechanical robustness via redox ions for flexible quasi-solid-state thermocells. *Nano Micro Lett*. 2022;14(1):81.

[18] Lei Z Y, Gao W, Zhu W Y, Wu P Y. Anti-fatigue and highly conductive thermocells for continuous electricity generation. *Adv. Funct. Mater.* 2022; 32: 2201021.

[19] Shi X F, Ma L, Li Y J, Shi Z P, Wei Q C, Ma G L, Zhang W W, Guo Y M, Wu P Y, Hu Z G. Double hydrogen-bonding reinforced high-performance supramolecular hydrogel thermocell for self-powered sensing remote-controlled by light. *Adv. Funct. Mater.*, 2023; 33: 2211720.

[20] Han C G, Qian X, Li Q K, Deng B, Zhu Y B, Han Z J, Zhang W Q, Wang W C, Feng S P, Chen G, Liu W S. Giant thermopower of ionic gelatin near room temperature. *Science*, 2020; 368: 1091-1098.

[21] Li Y C, Li Q K, Zhang X B, Zhang J J, Wang S H, Lai L Q, Zhu K, Liu W S. Realizing record-high output power in flexible gelatin/GTA-KCl-$FeCN^{4-/3-}$ ionic thermoelectric cells enabled by extending the working temperature range. *Energy Environ.*, *Sci.*2022; 15: 5379-5390.

[22] Yu B Y, Duan J J, Cong H J, Xie W K, Liu R, Zhuang X Y, Wang H,Qi B, Xu M, Wang Z L, Zhou J. Thermosensitive crystallization-boosted liquidthermocells for low-grade heat harvesting. *Science* 2020; 370: 342-346.

[23] Duan J J, Feng G, Yu B Y, Li J, Chen M, Yang P H, Feng J M, Liu K, Zhou J. Aqueous thermogalvanic cells with a high Seebeck coefficient for low-grade heat harvest. *Nat. Commun.*, 2018; 9:5146.